



SGM-101: An innovative near-infrared dye-antibody conjugate that targets CEA for fluorescence-guided surgery

Marian Gutowski ^{a,1}, Bérénice Framery ^{b,1}, Martin C. Boonstra ^c, Véronique Garambois ^{a,d,e,f}, François Quenet ^a, Karen Dumas ^b, François Scherninski ^g, Françoise Cailler ^b, Alexander L. Vahrmeijer ^c, André Pèlegrin ^{a,d,e,f,*}

^a Institut régional du Cancer de Montpellier, ICM, Montpellier, F-34298, France

^b SurgiMAb, 10 Parc Club du Millénaire, 1025 Avenue Henri Becquerel, 34000, Montpellier, France

^c Department of Surgery, Leiden University Medical Center, Leiden, The Netherlands

^d IRCM, Institut de Recherche en Cancérologie de Montpellier, Montpellier, F-34298, France

^e INSERM, U1194, Montpellier, F-34298, France

^f Université de Montpellier, Montpellier, F-34298, France

^g Laboratoires Synth-Innove, 2bis rue Dupont de l'Eure, 75020, Paris, France

ARTICLE INFO

Article history:

Received 14 December 2016

Received in revised form

6 January 2017

Accepted 6 March 2017

Keywords:

Immunophotodetection

Fluorescence-guided surgery

Digestive cancers

SGM-101

MAb-dye conjugates

ABSTRACT

Purpose: Fluorescence-guided surgery (FGS) provides surgeons with new opportunities to improve real-time cancer nodule detection and tumor margin visualization. Currently, the most important challenge in this field is the development of fluorescent dyes that specifically target tumors. We developed, characterized and evaluated SGM-101, an innovative antibody-dye conjugate in which the fluorochrome BM104, which has an absorbance band centered at 700 nm, is coupled to a chimeric monoclonal antibody (mAb) against carcinoembryonic antigen (CEA).

Methods: The dye to mAb ratio, binding to CEA and photobleaching of SGM-101 were determined. FGS was performed and results analyzed using different mouse models of human digestive tumors.

Results: SGM-101 allowed the detection of tumor nodules in three different colon cancer models: LS174T human colorectal adenocarcinoma cell-induced peritoneal carcinomatosis (PC) and liver metastases, and orthotopic grafts of HT29 human colorectal adenocarcinoma cells. In the PC model, submillimeter-sized nodules were detected during SGM-101-based FGS and SGM-101 predictive positive values ranged from 99.04% to 90.24% for tumor nodules >10 mg and nodules <1 mg, respectively. Similarly, in the orthotopic model of pancreatic cancer using BxPC3 (pancreas adenocarcinoma) cells, SGM-101 could clearly delineate tumors *in vivo* with a tumor-to-background ratio of 3.5, and penetrated in tumor nodules, as demonstrated by histological analysis. Free BM105 dye (BM104 with an activated ester for conjugation to the antibody) and an irrelevant conjugate did not induce any NIR fluorescence.

Conclusion: These preclinical data indicate that SGM-101 is an attractive candidate for FGS of CEA-expressing tumors and is currently assessed in clinical trials.

© 2017 The Authors. Published by Elsevier Ltd. This is an open access article under the CC BY-NC-ND license (<http://creativecommons.org/licenses/by-nc-nd/4.0/>).

1. Introduction

Digestive cancers are the most frequent and deadly tumors in both men and women (304 000 new cases and 153 000 deaths estimated for 2016 in the USA) [1]. Among them, colorectal cancer is the third most common cancer and leading cause of death in the USA [1]. In approximately 15% of patients with colorectal cancer, peritoneal carcinomatosis is already present at the time of diagnosis, and in 40% of patients, the disease is estimated to progress to peritoneal metastases after the initial diagnosis [2,3]. The extent of

Abbreviations: CEA, Carcinoembryonic antigen; mAb, monoclonal antibody; IPD, immunophotodetection; FGS, fluorescence image-guided surgery; NIR, near infrared; SPR, surface plasmon resonance; TBR, tumor to background ratio.

* Corresponding author. Institut de Recherche en Cancérologie de Montpellier, Campus Val d'Aurelle, Montpellier, F-34298, France.

E-mail address: andre.pelegrin@insERM.fr (A. Pèlegrin).

¹ These authors have contributed equally to the work.

peritoneal disease is often underestimated due to the low sensitivity and specificity of the current diagnostic tools (CT, MRI) in detecting small-size tumor nodules [4]. Currently, the most reliable diagnosis is obtained by direct observation through laparotomy or laparoscopy.

Until recently, peritoneal carcinomatosis was considered a terminal condition by most oncologists due to its very poor prognosis and was treated only with palliative care. In recent years, Sugarbaker et al. have introduced a new therapeutic approach that combines cytoreductive surgery, to remove all visible tumor deposits from the peritoneal surface, and hyperthermic intraperitoneal chemoperfusion, to target the microscopic residual disease [5,6]. This treatment strategy has drastically improved the primary and secondary prognosis of peritoneal carcinomatosis. The degree of macroscopic tumor resection is recorded using the completeness of cytoreduction (CCR) score (CCR-0 corresponds to absence of residual macroscopic peritoneal disease). Attaining a CCR-0 resection can significantly improve the 5-year survival rates of patients with colorectal cancer [7]. Therefore, powerful intra-operative imaging techniques are urgently needed to help achieving CCR-0 resection and for the accurate evaluation of tumor extension [8].

Pancreatic cancer is less frequent (around 53 000 new cases expected in the USA in 2016), but its mortality rate is very close to the incidence rate (42 000 expected deaths) [1]. New techniques to improve the current surgery outcomes should be developed, particularly to avoid positive resection margins that occur in 30% of patients [9].

Fluorescence imaging could provide surgeons with solutions to improve tumor resection thanks to the recent development of fluorescence-guided surgery (FGS) (see Refs. [10] and [11] for review). FGS becomes feasible because there are now several commercially available fluorescence image-guided surgery camera systems [11]. However, the currently approved dyes (fluorescein, methylene blue, ICG, IRD800CW) are non-targeted and/or are not in the near infrared (NIR) range, which is the optimum for *in vivo* applications [12]. High-performance NIR fluorescent targeted agents are required to provide surgeons with optimal guidance [13]. Monoclonal antibodies (mAbs) appear to be the best option to target NIR dyes [14]. Although it took more than twenty years to move from mice [15,16] to men and from pioneers' clinical work [17] to clinical studies, the translation of immunophotodetection (IPD; i.e., the use of dyes covalently linked to specific mAbs for the intra-operative detection of tumors) into the clinic seems now very close [18–21].

In the present study and as a first step toward clinical applications, we present the development and characterization of SGM-101, an innovative NIR reagent in which an original dye, BM104, is coupled to an anti-carcinoembryonic antigen (CEA) chimerized mAb. The good results obtained in different murine models of digestive cancers (orthotopic tumors, peritoneal carcinomatosis and hepatic metastases) and the results of extensive toxicological studies warrant a rapid clinical translation.

2. Materials and methods

2.1. Preparation and characterization of SGM-101 and control antibody-dye conjugates

The anti-CEA chimeric mAb SGM-ch511 was produced on a large scale (0.8 g/l) using a clinical compatible subclone of the CHO Protein-Free cell line (European Collection of Authenticated Cell Cultures, cat number 00102307) derived at Vivalis, France. Aliquots of 1 mg of SGM-ch511 in phosphate/bicarbonate buffer pH 9.3 were mixed with BM105 (BM104 with an activated ester for conjugation

to the antibody) or Alexa-Fluor 680 (AF680) dissolved in dimethylformamide (final concentration: 2.25 mg/ml) or with IRDye800-CW in bicarbonate buffer pH 8.5, at the indicated initial molar ratio. After agitation at 50 rpm at room temperature in the dark for 45 min, the dye-mAb conjugates were separated from free dye on PD-10 columns (GE Healthcare) equilibrated in elution buffer (10 mM KH₂PO₄, 10 mM Na₃Citrate, 300 mM Arginine, 0.02% (w/w) Tween-20, pH 6.0). The dye/mAb molar ratios were calculated using the mAb and dye molarities determined from optical density (OD) reading at 280 nm, 680 nm and 800 nm for AF680 ($\epsilon = 183\,000\text{ cm}^{-1}\cdot\text{M}^{-1}$) and IRDye800-CW ($\epsilon = 240\,000\text{ cm}^{-1}\cdot\text{M}^{-1}$) conjugates, respectively. For BM105 conjugates, the samples' absorbance was measured at 280 and 685 nm using a spectrophotometer (Jenway 7315, Bibby Scientific France) and then the labeling ratios were calculated using the following formula: Dye/protein = $(M_{\text{dye}})/((A_{280}/(0.3 \times \epsilon_{\text{protein}})/MW_{\text{protein}}))$, where the molar extinction coefficient of the protein ($\epsilon_{\text{protein}}$) was 1.5 M⁻¹ cm⁻¹, the molecular weight of the protein (MW_{protein}) was 150 000 g mol⁻¹. The molarity of the dye (M_{dye}) was calculated using the following formula: M_{dye} = $(A_{685\text{conjugate}} \times 10)/A_{685\text{dye}}$, where A_{685conjugate} was the absorbance of the conjugate at 685 nm and A_{685dye} was the absorbance of 10 µg of BM104 (diluted in the same buffer as the conjugate) at 685 nm.

A competitive ELISA was used to determine the CEA epitope recognized by SGM-ch511. Wells of a microtiter plate were coated with 1 µg/well recombinant CEA (Abcam) in PBS at 22 °C overnight. After washing with PBS and saturation with BSA 10 mg/ml in PBS, a fix quantity of SGM-ch511 (2.5 ng/well) mixed with dilutions (10 µg/ml to 1 ng/ml) of the reference mouse mAbs against the CEA epitopes Gold 1 to 5 (B93, 35A7, B17, CE25, and 192, respectively [22]) or the parental mAb 511 was added to the wells and incubated at 37 °C for 2 h. After washings, SGM-ch511 binding to CEA was revealed using peroxidase-labeled goat anti-human IgG and o-phenylenediamine dihydrochloride (OPD) followed by reading at 490 nm.

Quantum yield (QY) was measured according to Würth C et al. [23] using 5 µM of SGM-101, control conjugates and free dyes. After absorbance and fluorescence measurements, QY was calculated using the formula: $\phi_x = \phi_s (F_x/F_s) \times (f_s/f_x) \times (n_x^2/n_s^2)$, where ϕ_x was the sample QY, ϕ_s was the standard QY (= 0.39 for Alexa Fluor® 680 in PBS), F_x was the integrated intensity of fluorescence of the sample, F_s was the integrated intensity of fluorescence of the standard, f_s the absorption factor of the standard (= 1 – 10^{-Absorbance value}), f_x the absorption factor of the sample (= 1 – 10^{-Absorbance value}), n_x the refractive index of the sample buffer (e.g., n = 1.4305 for DMF, n = 1.334 for PBS) and n_s was the refractive index of the standard buffer (1.334 for PBS).

Photobleaching of the different conjugates (diluted to the same concentration) was measured after exposure to clinical wavelengths (i.e. wavelengths of the different devices approved for FGS). After exposure, fluorescence emission was registered with a spectrofluorimeter.

SGM-101 was radiolabeled with 2.5 µCi/µg ¹²⁵I by using the iodogen method (Pierce, Rockford, IL). Free ¹²⁵I was separated from labeled SGM-101 through a PD-10 column (GE Healthcare) equilibrated in PBS. The specific activity of the radiolabeled conjugate ranged from 1 to 2 µCi/µg. For binding analysis, 20 ng of ¹²⁵I-SGM-101 was mixed with CEA or an irrelevant antigen coupled to Sepharose beads and incubated at 37 °C with agitation overnight. The binding ratio was calculated using the following equation: cpm of the bound fraction (after bead washing)/cpm of the total fraction (before bead washing).

Mass spectrometry was performed using a 4800 Maldi TOF/TOF Analyzer (AB Sciex) and the 4000 Series Explorer™ software (AB Sciex). After dialysis against PBS just before analysis, diluted

samples (1:1 dilution in 10 mg/ml sinapinic acid in 0.1% TFA/50% acetonitrile, v/v) were loaded on the plate. Analysis was performed using the "High mass linear" method in positive mode, with an accelerating tension at source of 20 kV and a minimal accumulation of 3000 shootings/spectrum. Four measurements for each sample were carried out. The relative composition of the SGM-101 solution (antibody coupled to several dye molecules) was obtained by deconvolution of the main peak (corresponding to the sum of unique spectra) and by comparison with the reference peak obtained with the naked antibody.

The binding affinities of antibodies and conjugates for CEA were measured by surface plasmon resonance (SPR) using the BIACORE® technology (GE Healthcare). CEA was covalently immobilized on a CM5 sensor chip through thiol ligation, as recommended by the manufacturer (Surface Thiol Coupling GE Healthcare Instruction 22-0618-10AB). A control reference surface (flowcell Fc1), prepared using the same chemical treatment but without CEA injection, was used to measure the background signal. Five increasing concentrations (1.5–50 nM) of the parental mouse mAb 511, chimeric SGM-ch511 mAb and SGM-101 were used to determine the kinetic parameters and calculate the affinity constants.

2.2. Cell lines and nude mouse tumor models

The BxPC-3 (pancreas adenocarcinoma), LS-174T and HT29 (colorectal adenocarcinoma) human cell lines (ATCC) were cultured in RPMI-1640 medium with 10% fetal bovine serum in a humidified incubator at 37 °C and 5% CO₂. The BxPC-3-luc2 cell-line was purchased from PerkinElmer (MA, USA).

All animal experiments were performed in compliance with the French government guidelines and the Institut National de la Santé et de la Recherche Médicale regulations for experimental animal studies (agreement B34-172-27), or the "Code of Practice for the Use of Laboratory Animals in Cancer Research" (Inspectie W&V, July 1999, The Netherlands) with the approval of the relevant ethics committees in Montpellier, France, or Leiden, Netherlands. For tumor cell inoculation and image acquisition, animals were anesthetized with 4% isoflurane for induction and 2% isoflurane for maintenance.

Peritoneal carcinomatosis was induced by i.p. injection of 2.10⁶ LS174T cells in 150 µl serum-free culture medium in NMRI nude mice (Janvier, St Berthevin, France), as previously described [24]. Liver metastases were produced by intrasplicenic injection of 5.10⁵ LS174T cells in 50 µl serum-free culture medium through a 26-gauge needle, as described [25]. For the orthotopic colon cancer model, small fragments of subcutaneously growing HT29 tumors were transplanted in the cecum of nude mice, as described [26]. To induce subcutaneous tumors, BxPC-3 cells were injected at four sites on the back (500 000 cells per spot) [26]. Orthotopic pancreatic tumors were obtained as previously described by Kim et al. [27]. Following image acquisition, tumors were quickly frozen in isopentane for histological evaluation. Tumor growth in the orthotopic models was monitored weekly by bioluminescence imaging using luciferase-transfected cell lines, as previously described [26].

2.3. In vivo tumor localization of radiolabeled mAb-dye conjugates

Thirty µg of ¹²⁵I-SGM-101 were injected i.v. in nude mice with LS174T cell-derived peritoneal carcinomatosis. ¹²⁵I-SGM-101 uptake in the thyroid was limited by adding 0.05% iodine solution (Lugol) in the drinking water. To determine SGM-101 bio-distribution kinetics, groups of five mice were killed and dissected at different times (24 h, 48 h, 72 h and 96 h) after injection. The tumors and all organs were weighed and their ¹²⁵I radioactivity

measured using a gamma counter. Results were expressed as percentage of the injected dose (ID) per gram of tissue (%ID/g).

Whole-body SPECT images were acquired at 24 h, 48 h, 72 h and 96 h post-injection using a SPECT/CT imager (NanoSpect/CT, Bio-scan®). Mice were placed in prone position and scanned under anesthesia (1 l/min gas flow and 2% isoflurane in air). Helical CT scanning (45-keV) was followed by SPECT image acquisition (24 projections and 100s per projection). Imaging data were reconstructed iteratively with InVivoScope® and HiSPECT® for CT and SPECT, respectively.

2.4. NIR fluorescent imaging systems

Real-time NIR-fluorescence measurements and fluorescence-guided resections were performed using the FLARE™ NIR imaging system [26] or the V2IP system [28]. The Pearl Impulse small animal imaging system (LICOR, Bad Homburg, Germany) was used as an *in vivo* preclinical reference system to measure NIR fluorescent signals for biodistribution analysis and to calculate the tumor to background ratios (TBRs). Specific and control images were normalized and regions of interest were marked. The background signals were extracted from the surrounding tissue that was defined as the (normal) tissue/organ that lies around a tumor. After measuring the signal intensity of the macroscopic images, the TBR was calculated using the following formula: TBR = mean signal tumor/mean signal surrounding tissue.

2.5. Histological analysis

In the peritoneal carcinomatosis model, all biopsies and dissected tumor tissues were histologically analyzed after hematoxylin-eosin staining to determine the presence of tumor cells and to calculate the FGS performance parameters. For immunofluorescence analysis, imaging of 6-µm thick frozen tissue sections was performed using an Odyssey NIR scanner.

2.6. Statistical analysis

The histological results were compared with the fluorescence imaging data and reported in contingency tables. Sensitivity, specificity, and positive and negative predictive values (PPV and NPV) were then calculated [24]. Confidence limits were calculated from the binomial distribution.

3. Results

3.1. SGM-101 preparation and characterization

The innovative SGM-101 antibody-targeted fluorescent contrast agent is composed of two original molecules: the anti-CEA SGM-ch511 chimeric mAb and the fluorescent dye BM105 (the BM104 dye with an activated ester for conjugation to the antibody; see below for complete description) (Fig. 1A).

The mAb SGM-ch511 is the chimeric version of the mouse mAb 511 against the Gold 2 epitope of CEA [22]. Using five mAbs against the five Gold epitopes and mAb 511 in a competitive ELISA assay, we demonstrated that SGM-ch511 recognizes the same Gold epitope as the anti-Gold 2 mAb (Fig. 1B). SGM-ch511 affinity for CEA (3.27×10^{-11} M) remained very close to that of the parental murine mAb 511 (3.82×10^{-11} M) and was not significantly modified upon labeling with BM105 (3.21×10^{-11} M), as indicated by the SPR results using a CEA-coated chip.

To determine the best BM104/mAb molar ratio, eight conjugates were synthesized with an initial molar ratio between 3 and 20, which gave a final molar ratio between 1 and 4.5, respectively

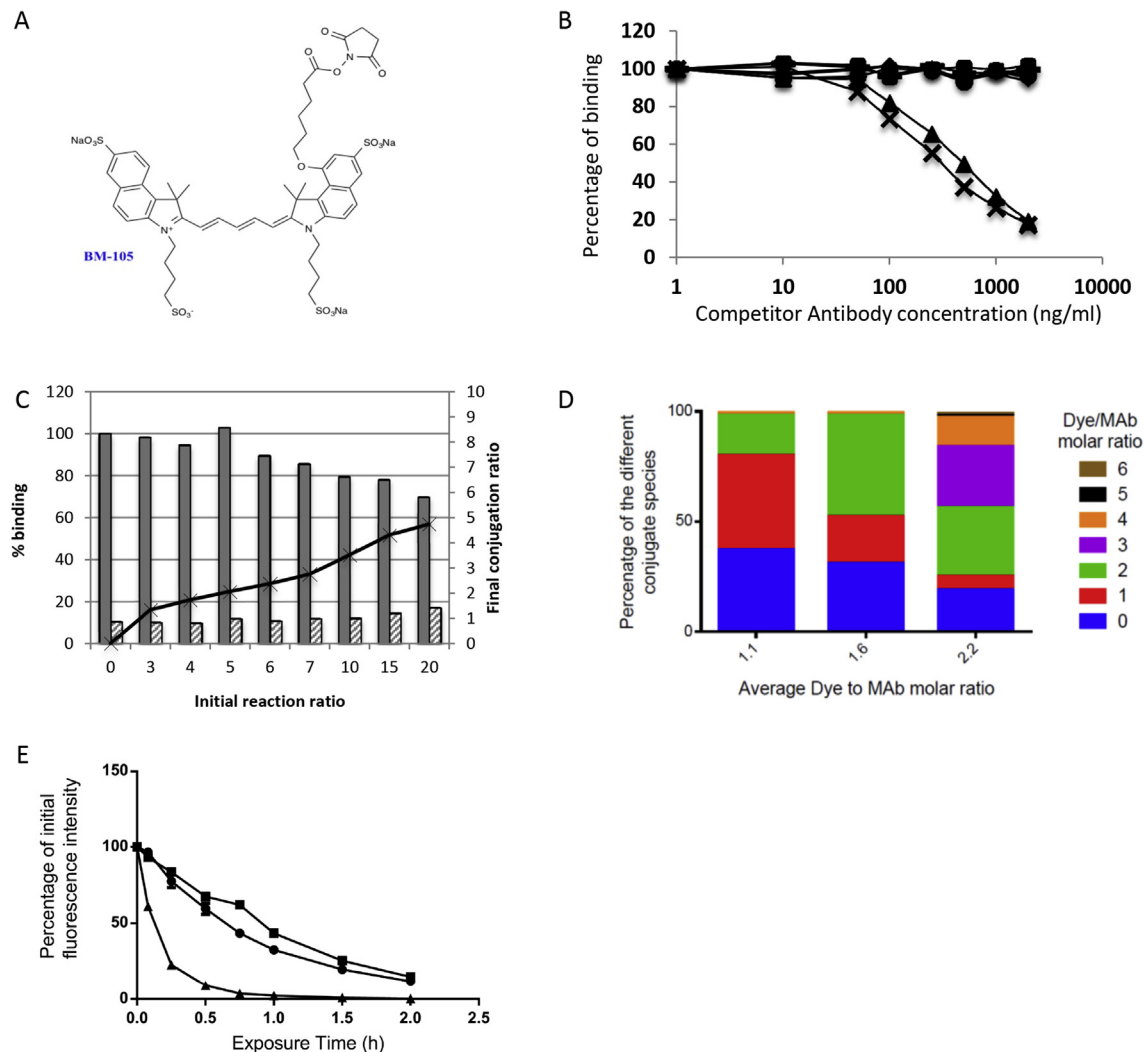


Fig. 1. BM105 and SGM-101 characterization. A: Extended formula of the BM105 dye; B: Competitive ELISA assay showing that the binding of the chimeric antibody SGM-ch511 to CEA is inhibited by its parental murine mAb 511 (▲) and a reference mAb directed against the Gold 2 CEA epitope (×), but not by reference mAbs against the Gold 1 (■), 3 (●), 4 (◆) and 5 (○) CEA epitopes; C: Final conjugation ratios (curve) of BM104-SGM-ch511 conjugates, depending on the initial molar ratio, and their binding percentage to CEA (gray bars) and to an irrelevant antigen (striped bars); D: Mass spectroscopy analysis of three SGM-101 batches to determine the percentage of each form; E: Photobleaching measurement of SGM-101 (●), SGM-ch511-AF680 (▲) and SGM-ch511-IRDye800-CW (■).

(Fig. 1C). The specific binding of radiolabeled SGM-101 to CEA was higher than 90%, when the conjugate contained up to three BM104 molecules per mAb molecule. With higher dye loads, the specific binding to CEA decreased and the non-specific binding (to the irrelevant Ag) increased (Fig. 1C). Therefore, a final dye to mAb molar ratio between 1 and 2 was chosen for all other experiments. The average final dye to mAb molar ratio was determined using absorption at 280 nm and 685 nm. A more precise analysis using mass spectrometry provided the exact percentage of each form in the final product (Fig. 1D). For example, a SGM-101 batch with an average dye/mAb ratio of 1.6 included 31, 21, 46 and 2% of conjugate with a dye/mAb ratio of 0, 1, 2 and 4, respectively (Fig. 1D). In comparison, a conjugate with an average dye/mAb ratio of 1.1 contained 43% of SGM-101 with a 1/1 ratio, whereas a conjugate with an average dye/mAb ratio of 2.2 contained about one third of SGM-101 with three BM104 molecules per SGM-ch511 molecule.

The BM105 NIR dye is composed of BM104, a fluorescent carbocyanine dye with an activated ester that allows its conjugation to the antibody (Fig. 1A). This fluorophore was specifically developed to minimize the aggregation risk during the coupling reaction with

a biological substrate and consequently to improve the optical and labeling properties. BM105 absorbance peak was at 685 nm with a good absorbance from 670 to 700 nm (about 70% of the 685 nm maximum) and the fluorescence peak was at 705 nm. This allows stimulation and detection using the “700 nm version” of the available clinical devices (FLARE™ and Fluobeam; $\lambda_{ex} = 660$ and 680 nm, respectively; λ for detection = 689–725 nm and > 700 nm, respectively). The absorption and fluorescence of free BM105 and antibody-linked BM104 were not significantly different (data not shown). Based on the protocol provided by Würth C et al. [23], the fluorescence QY of SGM-101 and of BM105 were measured and compared to the QY of AF680 and IRDye800-CW, as free dyes or conjugated with the SGM-ch511 mAb. AF680 was chosen because its excitation wavelength is close to that of BM105 and IRDye800-CW because it is the only dye which has been tested in clinical trials [29]. BM105 QY values were 0.22 and 0.17 for the free and conjugated forms, respectively. These values were very close to those of AF680 (QY = 0.42 and 0.33, free and conjugated forms, respectively) and much higher than those of IRDye800-CW (QY = 0.05 and 0.02, free and conjugated forms, respectively).

Comparison of the photobleaching characteristics of the three conjugates (Fig. 1E) showed that SGM-101 was very stable (67% and 31% of the initial fluorescence at 30 and 60 min, respectively). SGM-ch511-IRDye800-CW gave similar results, while SGM-ch511-AF680 was very unstable with only 22% of the initial fluorescence left at 15 min (Fig. 1E). In summary, when compared with SGM-ch511-AF680 and SGM-ch511-IRDye800-CW, SGM-101 was the only conjugate that associated high QY and low photobleaching up to 1 h (a time period fully compatible with FGS).

3.2. SGM-101 for the detection of colon cancer peritoneal carcinomatosis: biodistribution studies of ^{125}I -SGM-101, SPECT-CT imaging and immunophotodetection

SGM1-101 was first evaluated in a mouse model of peritoneal carcinomatosis induced by i.p. injection of LS174T colorectal

adenocarcinoma cells. To determine precisely SGM1-101 bio-distribution, mice with peritoneal carcinomatosis were sacrificed at different time points (24 h–96 h) after i.v. injection of 30 μg ^{125}I -SGM-101 (Fig. 2A). Tumor uptake at 24 h post-injection was $14.35 \pm 0.87\%$ ID/g tumor and the maximal tumor uptake ($23.73 \pm 5.42\%$ ID/g) was reached at 48 h. Tumor uptake was still up to $10.15 \pm 4.76\%$ ID/g tumor at 72 h. The tumor-to-normal tissue ratios ranged from 2.40 ± 0.27 , 3.89 ± 0.90 , 2.81 ± 0.2 and 3.87 ± 0.89 for blood at 24, 48, 72 and 96 h, respectively, to 27.19 ± 3.70 , 31.65 ± 4.03 , 34.93 ± 7.41 and 36.96 ± 5.16 for muscle. Intermediate values of 5.41 ± 0.68 , 9.40 ± 3.11 , 8.60 ± 2.14 and 9.54 ± 2.16 were observed in liver at the same time points after injection. ^{125}I -SGM-101 uptake in tumor nodules was also monitored using SPECT-CT imaging (Fig. 2B).

Based on this biodistribution kinetics, FGS was performed in eight mice with LS174T cell-induced peritoneal carcinomatosis 48 h

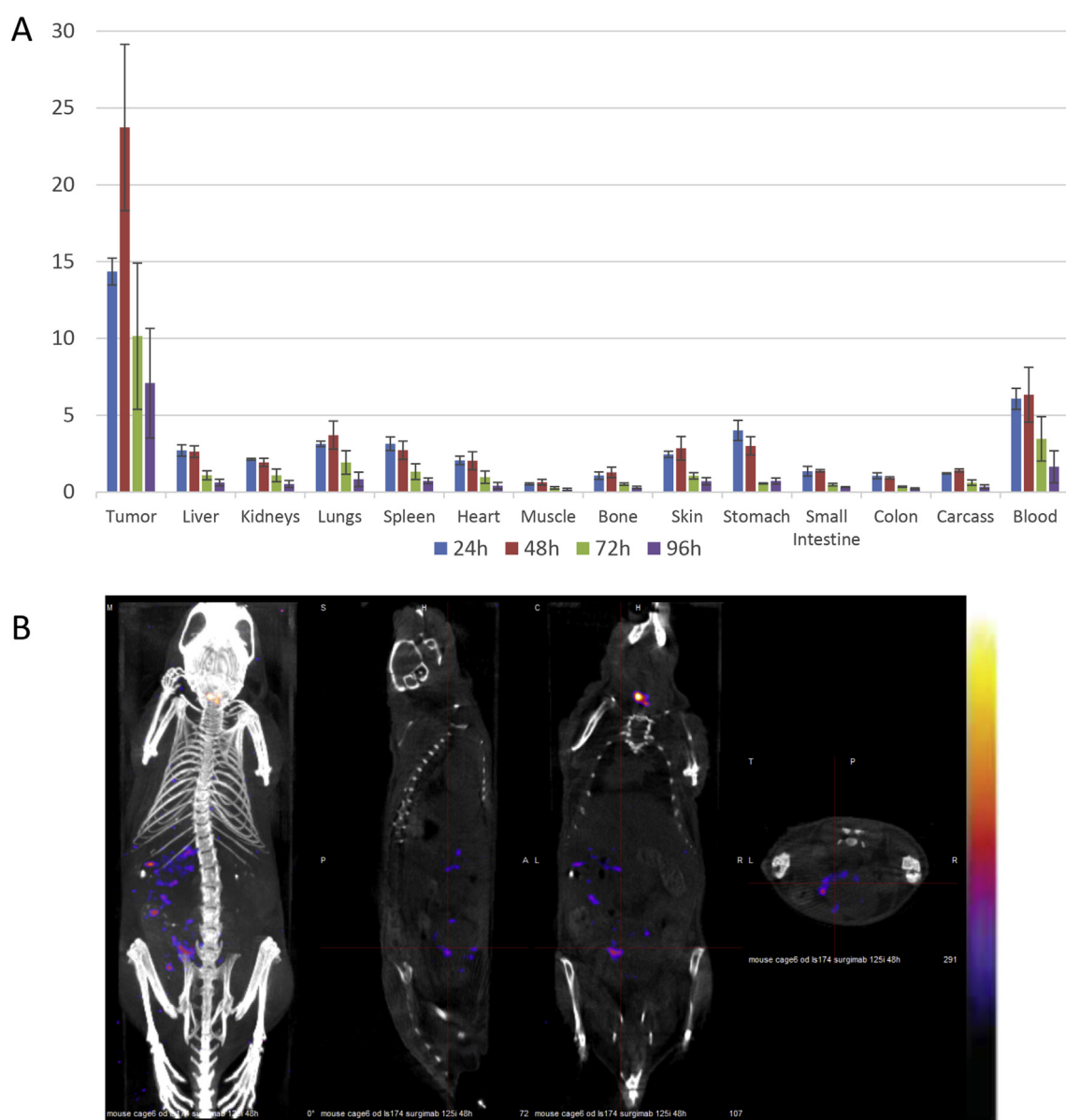


Fig. 2. Biodistribution studies of ^{125}I -SGM-101 in nude mice with LS174T cell-derived peritoneal carcinomatosis. A: Analysis of radioactivity distribution in nude mice with LS174T cell-derived peritoneal carcinomatosis at 24, 48, 72 and 96 h after i.v. injection of 30 μg of ^{125}I -SGM-101. The % ID/g of tissue was determined by measuring the radioactivity in each organ. B: SPECT-CT images showing ^{125}I -SGM-101 uptake by nodules in mice with LS174T cell-derived peritoneal carcinomatosis at 48 h after injection. From left to right: planar, sagittal, frontal and transversal views.

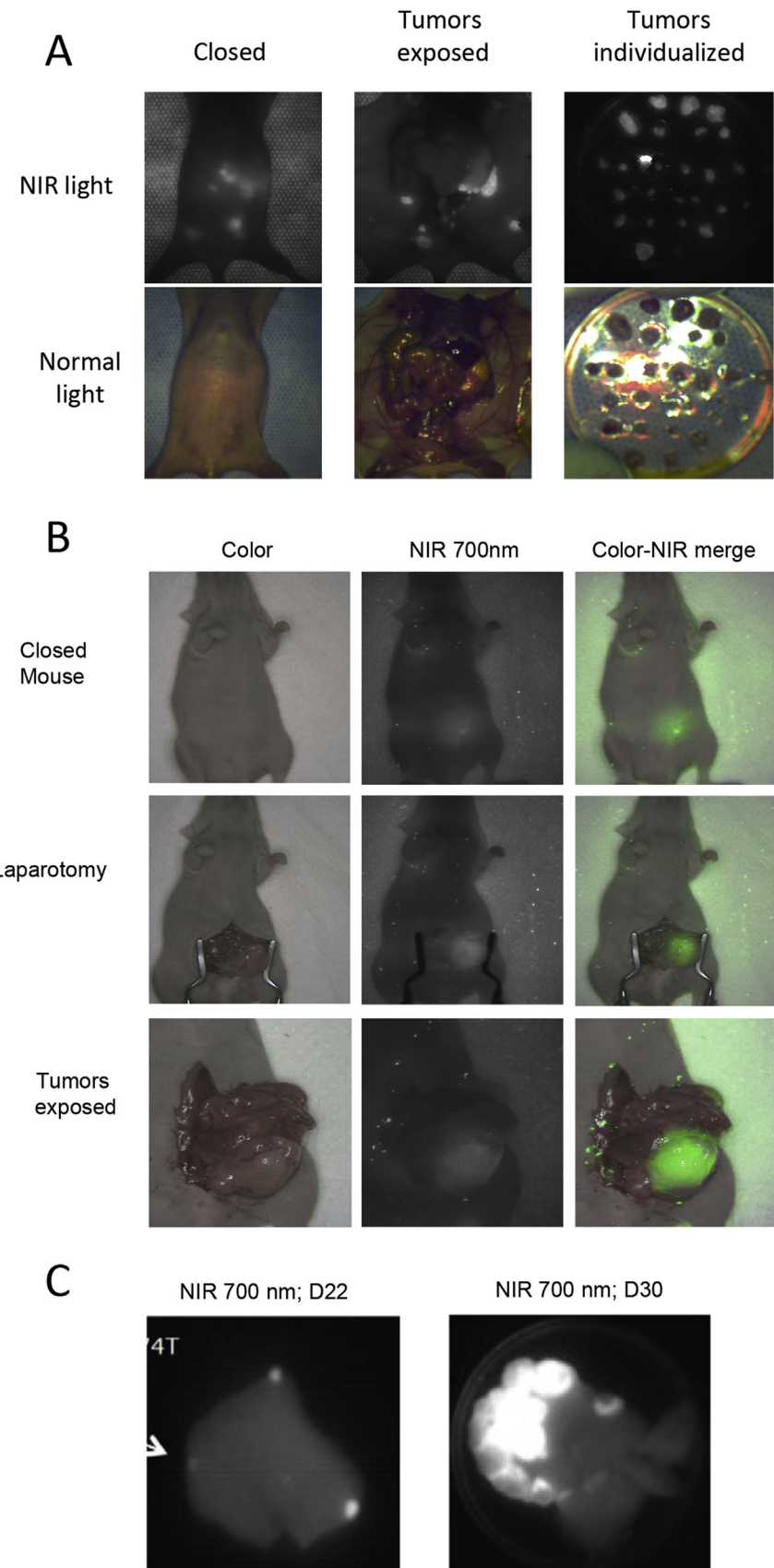


Fig. 3. Immunophotodetection of tumor nodules in three mouse models of colon cancer. Animals were imaged under normal (color) or NIR light 48 h after i.v. injection of 30 µg of SGM-101. A: LS174T cell-derived peritoneal carcinomatosis (V2IP imaging system); B: Orthotopic colon cancer model using HT29 cells (FLARE™ NIR imaging system); C: LS174T cell-derived liver metastases obtained at day 22 (D22) and D30 after cell inoculation (V2IP imaging system).

after i.v. injection of 30 µg of SGM-101. For the largest tumor nodules (> 10 mg), fluorescence could already be detected through the skin before laparotomy (Fig. 3A). During laparotomy, a careful analysis of the whole peritoneum allowed the resection of very small tumor nodules that would not have been detected without the antibody-targeted fluorescent dye (Fig. 3A).

In addition to the resection of all detectable fluorescent nodules, biopsies of diaphragm, mesocolon, mesentery, omentum and Douglas pouch were systematically performed. Their histological analysis allowed calculating SGM-101-based FGS sensitivity, specificity, PPV and NPV (Table 1). Fluorescent nodules ($n = 312$) were divided in three groups according to their weight (≤ 1 mg; > 1 and ≤ 10 mg; ≥ 10 mg) to analyze the influence of the tumor size on FGS sensitivity (Table 1B). The tumor nature of all fluorescent nodules > 10 mg, but one (99% PPV), was confirmed by histological analysis. For nodules < 1 mg, PPV was still high (90.24%). These results confirmed SGM-101 capacity to target very small (sub-millimeter sized) tumor nodules and to make them detectable for FGS.

3.3. SGM101 allows the visualization of orthotopic colon cancer grafts, liver metastases and pancreatic tumor cell xenografts

Besides peritoneal carcinomatosis of digestive cancers, SGM-101 could be an attractive fluorescent tracer for FGS of colorectal and pancreatic carcinomas. SGM-101 performances were therefore analyzed in orthotopic tumor models because they are closer to the clinical situation than subcutaneous tumor cell grafts. The dose of 30 µg SGM-101 and the 48 h delay between injection and IPD were kept constant in all these experiments. The results obtained in the pancreatic cancer model will be described more in detail.

First, in the orthotopic colon cancer model using HT29 cells, mice injected with SGM-101 showed a bright fluorescence nodule that was clearly demarcated from the surrounding tissue (Fig. 3B). The largest nodules were detectable before laparotomy. Second, liver metastases could be detected about 3 weeks after intra-splenic injection of LS174T colorectal adenocarcinoma cells (Fig. 3C). Smaller than 1 mm³ nodules, which were undetectable by visual inspection or palpation, were fluorescent and their tumor

nature was confirmed by histological analysis (data not shown). Larger LS174T cell nodules also were fluorescent (Fig. 3C). Third, the orthotopic pancreatic cancer model using BxPC3-luc2 cells allowed demonstrating that SGM-101-induced fluorescence co-localized with luciferase-positive tumor cells (Fig. 4A). The need of a tumor-specific conjugate was confirmed by comparing SGM-101 with an irrelevant conjugate (at the same dose as SGM-101, 30 µg) and with free BM105 (250 ng; this dose corresponds to the quantity of BM105 contained in 30 µg of SGM-101). BM105 and the irrelevant conjugate did not induce any tumor-associated fluorescence (Fig. 4A). Using the FLARE™ imaging system, a TBR of 3.5 ± 0.6 was calculated for SGM-101-injected mice, compared with 1.2 ± 0.5 and 1.0 ± 0.1 for mice injected with BM105 or the irrelevant conjugate, respectively (Fig. 4B). After imaging, orthotopic pancreatic tumors were excised and snap-frozen. Consecutive pancreatic tumor tissue sections were imaged to evaluate the distribution of the fluorescent signal, or stained with hematoxylin and eosin to confirm the presence of human tumor cells. The localization of the fluorescent signal and of tumor cells was remarkably similar (Fig. 4C).

4. Discussion

FGS is moving rapidly into the clinic and there is a consensus between experts that the current limiting factor, particularly in oncology, is the fluorescent agent [10,11,13,29]. Indeed, although there is still some room for improvement, several optical devices have been developed and marketed (e.g., QUEST medical imaging and Fluoptics) thanks to the active research and development in recent years [30,31]. Concerning targeting agents, fluorescent dyes conjugated with specific mAbs can combine exquisite tumor specificity and optimal fluorescence performances [15–20,26,32,33]. Here, we describe SGM-101, an innovative conjugate that combines the specific tumor-targeting properties of an anti-CEA mAb with an optimal fluorescent dye (BM104).

Thanks to the use of mAbs as therapeutic agents, all the issues concerning their development, large production according to good manufacturing practices and related costs have been already overcome [34]. More precisely concerning SGM-101, the SGM-ch511 mAb production yields were about 0.8–1 g/l at the clinical grade in CHO and the conjugation process with BM105 was robust enough to be performed with batches of several grams of mAb. These good production conditions together with a planned low injected dose (several mg, see below for details) should allow the commercialization of SGM-101 at an affordable price. The most important remaining question is the target antigen to be used in FGS. For many years, radiolabeled anti-CEA antibodies have been evaluated and used in the clinic for imaging and therapy. However, up to now, their potential did not translate into marketed and routinely used reagents [35–38]. CEA is one of the most relevant target antigens for FGS because it is expressed in almost all digestive cancers and in most breast cancers at high antigenic density [39]. Its expression at the cell surface is stable and constant from primary tumors to all types of metastases. For these reasons, several groups are interested in evaluating anti-CEA/dye conjugates to develop tools for FGS of digestive cancers [15–17,26,32,33]. For other pathologies, some authors have been using already approved therapeutic mAbs, despite their limited relevance for FGS [18–20]. Indeed, the antigens targeted by these mAbs are not widely expressed (e.g., HER2 only in 30% of breast cancers) or not at the membrane (e.g., VEGF), or they are also strongly expressed in normal tissues (e.g., EGFR that also shows variable expression in tumors). The high CEA antigenic density (10^5 to 10^6 antigens per cell) in most cancers is an important success factor for FGS [40]. With such an antigenic density, one can expect to achieve a dye

Table 1
FGS performance parameters in the LS174T cell-derived peritoneal carcinomatosis model.

A. Fluorescent nodules and non-fluorescent biopsies of diaphragm, mesocolon, mesentery, omentum and Douglas pouch			
	Presence of tumor		
	Yes	No	
Fluorescence			Confidence limits (95%)
Yes	302	10	95.8–99.3
No	6	39	65.7–89.8
Sensitivity	98.05		94.2–98.5
Specificity	79.59		86.67
PPV	96.79		73.3–94.9
NPV			90.24
B: Results of histological analysis of fluorescent nodules subdivided according to their weight			
Nodule weight	Presence of tumor	PPV	Confidence limits (95%)
	Yes	No	
>10 mg	103	1	99.04
10 mg > nodule > 1 mg	162	5	97.01
<1 mg	37	4	90.24

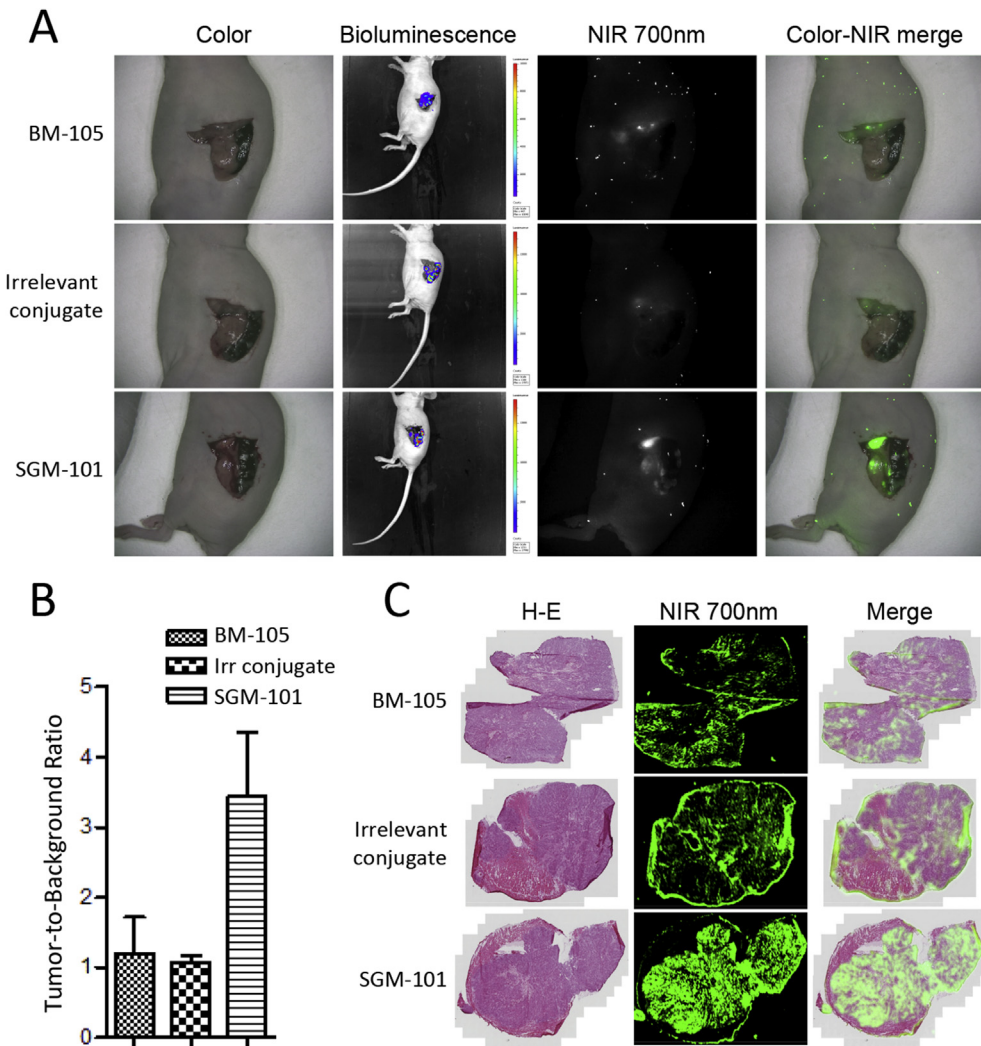


Fig. 4. Immunophotodetection of tumors in a mouse orthotopic model of pancreatic cancer using BxPC3 cells. A: Animals with orthotopic BxPC3 cell-derived tumor xenografts were sacrificed 48 h after i.v. injection of 250 ng of BM105 dye, 30 µg of non-specific (irrelevant) conjugate or 30 µg of SGM-101. Images were acquired using the Pearl Impulse small animal imaging system for bioluminescent detection of tumor cells (Bioluminescence) and with the FLARE™ NIR imaging system for fluorescence visualization at 700 nm (NIR). B: The tumor to background ratio was calculated using the formula: TBR = mean signal tumor/mean signal surrounding tissue using the signal intensity for each tissue measured with the Pearl Impulse imaging system. C: Histologic and immunofluorescence analyses of BxPC3 cell-derived tumor xenografts showing that the fluorescence signal is only observed in tumors from mice injected with SGM-101.

concentration of up to 1 µM assuming a 1:1 ratio of targeted dye per receptor ([10,41] and personal computations). This corresponds to the maximal calculated concentration and the SGM-101 high affinity for CEA (3.21×10^{-11} M) should make possible to be close to it. The present study focused on digestive cancers; however, CEA is expressed in 65% of breast cancers [42] and obtaining clear margins is very important, especially during breast-sparing surgery [43]. Therefore, FGS using SGM-101 could be useful also in this setting.

When coupled to SGM-ch511, BM104 compared favorably with AF680, a dye with similar excitation and emission wavelengths, and with IRDye800-CW the only dye that can be coupled to mAbs and has been used in clinical trials. SGM-101 was the only conjugate with high QY and low photobleaching for a time period compatible with FGS (Fig. 1). BM104 was centered on 700 nm (λ_{ex} 685 nm, λ_{em} 705 nm) for several reasons: (i) at 700 nm, the maximum penetration of light in live tissues (around 10 mm) is already achieved [30]; (ii) at 700 nm, the quantum efficiency of the camera is higher than at 800 nm where it can be $\leq 25\%$ [13,31]; (iii) with a tumor-targeting agent centered on 700 nm, a non-specific dye centered

on 800 nm, such as ICG, can be concomitantly used for analysis of normal tissue functions or reconstructive surgery [44].

In imaging, there has been a tendency to use mAb fragments, such as single-chain variable fragments (scFv) [26,45] or nanobodies [46,47], based on the argument that a short kinetics is more favorable and that small entities can penetrate more deeply in tumor nodules. Nevertheless, here we show by immunofluorescence analysis of orthotopic BxPC3 tumors that SGM-101 can penetrate in submillimeter-sized tumor nodules and give a homogeneous tumor uptake (Fig. 4C). Moreover, the use of intact mAbs is fully compatible with clinical constraints. Indeed, thanks to their longer half-life (compared with antibody fragments), intraoperative imaging using dye-intact mAb conjugates can be performed during a longer period of time after injection. For example, preliminary data from an open clinical trial using cetuximab-IRDye 800CW show that surgery can be performed within 2–5 days after injection (NCT02736578). Finally, the core chemical compound that absorbs and emits in the near-infrared is necessarily large and hydrophobic [13]. By using intact mAbs, the potential hydrophobicity of the dye

has a limited effect on the conjugate hydrophilicity. In the present work, we demonstrate that SGM-101, which contains an average of 1.6 BM104 molecules per mAb molecule, behaves like the unconjugated SGM-ch511 mAb with no major accumulation in normal tissues. Conversely, when using an anti-CEA disulfide-stabilized scFv coupled to IRDye800-CW (ssSM3E/800CW), accumulation also in liver and kidney was observed in the BxPC3 cell-derived orthotopic pancreatic cancer model [26]. In the same orthotopic pancreatic tumor model, the maximal TBR was 3.5 ± 0.9 for SGM-101 (Fig. 4C) and 2.37 ± 0.4 for ssSM3E/800CW [26] at 48 h and 24 h post-injection, respectively.

For SGM-101 clinical translation, some issues need to be solved, particularly: (i) the administration route (i.v. vs topical) and, in the case of i.v. injection, the delay between administration and surgery; and (ii) the dose to be injected. Topical spraying is claimed to be the simplest way to administer targeted agents for FGS [48]. However, topically administered compounds can only highlight the structures at the surface of which they are applied. Conversely, injectable drugs can highlight structures below the surface, thus directing the surgeon to structures that they have not seen by naked eye [11]. We and others [11] are convinced that this topographically unbiased ability to highlight the structures of interest is superior for surgical applications. When mAb-dye conjugates are used, the kinetic parameters also need to be considered because optimal antibody binding to its cognate antigen is not immediate [49]. Here again, i.v. injection is more favorable than topical administration. The injected dose and the interval between injection and surgery should allow optimal binding and consequently a clear visualization of tumor nodules without any significant background signal, due to circulating conjugate. In our mouse model of peritoneal carcinomatosis, the maximum tumor uptake was at 24 h (Fig. 2A). As mAb kinetics are slower in humans, a larger time window, between 24 h and 96 h, should be considered for FGS after i.v. injection.

The choice of dose to be used is not an easy task because FSG is a multi-parametric approach and the results depend on the targeted antigen, the fluorescent dye-mAb conjugate and the imaging device performances. When using conventional strategies to convert animal doses to human-equivalent doses, such as those based on the body surface area [50], the SGM-101 dose of 30 µg for a mouse weighing 20 g corresponds to about 10 mg for a human patient of 80 kg. For mAb-targeted dyes, the dose could also be chosen on the basis of previous imaging studies using radiolabeled antibodies. Such approach gives doses in the same range as those obtained based on the body surface area [37]. Such dose calculation depends also on the target antigen. Only CEA expressed by the tumor nodule can be accessed by i.v. injected mAbs because all CEA expressed on the apical side of normal colon cannot be reached [37]. Based on these different methods, doses between 5 and 15 mg should be used in future clinical trials. With antibodies against more ubiquitous antigens, such as EGFR, higher doses need to be used to compensate for the uptake by normal organs (up to 62.5 mg/m^2 ; i.e., more than 100 mg per injection in the first clinical trial of cetuximab-IRDye800 in head and neck cancers [51]).

Based on the present preclinical data using different mouse models of digestive cancers, extensive regulatory toxicological studies were performed and confirmed that SGM-101 is safe for human use (manuscript in preparation). Clinical trials are now in progress in patients with digestive cancer peritoneal carcinomatosis, pancreatic cancer or rectum cancer.

Conflicts of interest

FC, BF, KD are employed by SurgiMAb that owns the SGM-101 conjugate.

FC, AP, MG are part of SurgiMAb founders and stockholders.

FS is CEO of Synth>Innove that developed and patented the BM105 dye.

The other authors declare no conflict of interest.

Acknowledgements

We would like to thank H.A.J.M Prevoo for her immunohistochemical expertise, Caroline Mollevi for statistical analysis, Martine Pugnière and Corinne Henriet for SPR experiments, Christian Larroque and Nicole Bec for mass spectroscopy, Muriel Busson for SPECT-CT imaging. This work was supported by grants from SurgiMAb.

References

- [1] R.L. Siegel, K.D. Miller, A. Jemal, Cancer statistics, 2016, CA, Cancer J. Clin. 66 (2016) 7–30, <http://dx.doi.org/10.3322/caac.21332>.
- [2] M.J. Koppe, O.C. Boerman, W.J.G. Oyen, R.P. Bleichrodt, Peritoneal carcinomatosis of colorectal origin: incidence and current treatment strategies, Ann. Surg. 243 (2006) 212–222, <http://dx.doi.org/10.1097/01.sla.0000197702.46394.16>.
- [3] T.C. Chua, J. Esquivel, J.O.W. Pelz, D.L. Morris, Summary of current therapeutic options for peritoneal metastases from colorectal cancer, J. Surg. Oncol. 107 (2013) 566–573, <http://dx.doi.org/10.1002/jso.23189>.
- [4] Y.L.B. Klaver, V.E.P.P. Lemmens, S.W. Nienhuis, M.D.P. Luyer, I.H.J.T. de Hingh, Peritoneal carcinomatosis of colorectal origin: incidence, prognosis and treatment options, World J. Gastroenterol. WJG 18 (2012) 5489–5494, <http://dx.doi.org/10.3748/wjg.v18.i39.5489>.
- [5] P.H. Sugarbaker, Peritonectomy procedures, Ann. Surg. 221 (1995) 29–42.
- [6] F. Quenet, D. Goéry, S.S. Mehta, L. Roca, F. Dumont, M. Hessissen, B. Saint-Aubert, D. Elias, Results of two bi-institutional prospective studies using intraperitoneal oxaliplatin with or without irinotecan during HIPEC after cytoreductive surgery for colorectal carcinomatosis, Ann. Surg. 254 (2011) 294–301, <http://dx.doi.org/10.1097/SLA.0b013e3182263933>.
- [7] O. Glehen, F. Kwiatkowski, P.H. Sugarbaker, D. Elias, E.A. Levine, M. De Simone, R. Barone, Y. Yonemura, F. Cavaliere, F. Quenet, M. Gutman, A.a.K. Tentes, G. Lorimier, J.L. Bernard, J.M. Bereder, J. Porcheron, A. Gomez-Portilla, P. Shen, M. Deraco, P. Rat, Cytoreductive surgery combined with perioperative intraperitoneal chemotherapy for the management of peritoneal carcinomatosis from colorectal cancer: a multi-institutional study, J. Clin. Oncol. Off. J. Am. Soc. Clin. Oncol. 22 (2004) 3284–3292, <http://dx.doi.org/10.1200/JCO.2004.10.012>.
- [8] H. Orbay, J. Bean, Y. Zhang, W. Cai, Intraoperative targeted optical imaging: a guide towards tumor-free margins in cancer surgery, Curr. Pharm. Biotechnol. 14 (2013) 733–742.
- [9] D.A. Ruess, F. Makowiec, S. Chikhladze, O. Sick, H. Riediger, U.T. Hopt, U.A. Wittel, The prognostic influence of intrapancreatic tumor location on survival after resection of pancreatic ductal adenocarcinoma, BMC Surg. 15 (2015) 123, <http://dx.doi.org/10.1186/s12893-015-0110-5>.
- [10] A.L. Vahrmeijer, M. Hutteman, J.R. van der Vorst, C.J.H. van de Velde, J.V. Frangioni, Image-guided cancer surgery using near-infrared fluorescence, Nat. Rev. Clin. Oncol. 10 (2013) 507–518, <http://dx.doi.org/10.1038/nrclinonc.2013.123>.
- [11] Q.T. Nguyen, R.Y. Tsien, Fluorescence-guided surgery with live molecular navigation—a new cutting edge, Nat. Rev. Cancer 13 (2013) 653–662, <http://dx.doi.org/10.1038/nrc3566>.
- [12] G.M. van Dam, G. Themelis, L.M.A. Crane, N.J. Harlaar, R.G. Pleijhuis, W. Kelder, A. Sarantopoulos, J.S. de Jong, H.J.G. Arts, A.G.J. van der Zee, J. Bart, P.S. Low, V. Ntziachristos, Intraoperative tumor-specific fluorescence imaging in ovarian cancer by folate receptor- α targeting: first in-human results, Nat. Med. (2011), <http://dx.doi.org/10.1038/nm.2472>.
- [13] S. Gioux, H.S. Choi, J.V. Frangioni, Image-guided surgery using invisible near-infrared light: fundamentals of clinical translation, Mol. Imaging 9 (2010) 237–255.
- [14] K.D. Wittrup, G.M. Thurber, M.M. Schmidt, J.J. Rhoden, Practical theoretic guidance for the design of tumor-targeting agents, Methods Enzymol. 503 (2012) 255–268, <http://dx.doi.org/10.1016/B978-0-12-396962-0.00010-0>.
- [15] A. Péligrin, S. Folli, F. Buchegger, J.P. Mach, G. Wagnières, H. van den Bergh, Antibody-fluorescein conjugates for photoimmunodiagnosis of human colon carcinoma in nude mice, Cancer 67 (1991) 2529–2537.
- [16] S. Folli, P. Westermann, D. Braichotte, A. Péligrin, G. Wagnières, H. van den Bergh, J.P. Mach, Antibody-indocyanin conjugates for immunophotodetection of human squamous cell carcinoma in nude mice, Cancer Res. 54 (1994) 2643–2649.
- [17] S. Folli, G. Wagnières, A. Péligrin, J.M. Calmes, D. Braichotte, F. Buchegger, Y. Chalandon, N. Hardman, C. Heusser, J.C. Givel, Immunophotodiagnosis of colon carcinomas in patients injected with fluoresceinated chimeric antibodies against carcinoembryonic antigen, Proc. Natl. Acad. Sci. U. S. A. 89 (1992) 7973–7977.
- [18] A.G.T. Terwisscha van Scheltinga, G.M. van Dam, W.B. Nagengast,

- V. Ntziachristos, H. Hollema, J.L. Herek, C.P. Schröder, J.G.W. Kosterink, M.N. Lub-de Hoog, E.G.E. de Vries, Intraoperative near-infrared fluorescence tumor imaging with vascular endothelial growth factor and human epidermal growth factor receptor 2 targeting antibodies, *J. Nucl. Med. Off. Publ. Soc. Nucl. Med* 52 (2011) 1778–1785, <http://dx.doi.org/10.2967/jnumed.111.092833>.
- [19] C.H. Heath, N.L. Deep, L. Sweeny, K.R. Zinn, E.L. Rosenthal, Use of panitumumab-IRDye800 to image microscopic head and neck cancer in an orthotopic surgical model, *Ann. Surg. Oncol.* 19 (2012) 3879–3887, <http://dx.doi.org/10.1245/s10434-012-2435-y>.
- [20] M.L. Korb, Y.E. Hartman, J. Kovar, K.R. Zinn, K.I. Bland, E.L. Rosenthal, Use of monoclonal antibody-IRDye800CW bioconjugates in the resection of breast cancer, *J. Surg. Res.* 188 (2014) 119–128, <http://dx.doi.org/10.1016/j.jss.2013.11.1089>.
- [21] N.J. Harlaar, M. Koller, S.J. de Jongh, B.L. van Leeuwen, P.H. Hemmer, S. Kruijff, R.J. van Ginkel, L.B. Been, J.S. de Jong, G. Kats-Ugurlu, M.D. Linszen, A. Jorritsma-Smit, M. van Oosten, W.B. Nagengast, V. Ntziachristos, G.M. van Dam, Molecular fluorescence-guided surgery of peritoneal carcinomatosis of colorectal origin: a single-centre feasibility study, *Lancet Gastroenterol. Hepatol.* 1 (n.d.) 283–290, [10.1016/S2468-1253\(16\)30082-6](http://dx.doi.org/10.1016/S2468-1253(16)30082-6).
- [22] S. Hammarstrom, J.E. Shively, R.J. Paxton, B.G. Beatty, A. Larsson, R. Ghosh, O. Bormer, F. Buchegger, J.P. Mach, P. Burtin, Antigenic sites in carcinoembryonic antigen, *Cancer Res.* 49 (1989) 4852–4858.
- [23] C. Würth, M. Grabolle, J. Pauli, M. Spieles, U. Resch-Genger, Relative and absolute determination of fluorescence quantum yields of transparent samples, *Nat. Protoc.* 8 (2013) 1535–1550, <http://dx.doi.org/10.1038/nprot.2013.087>.
- [24] M. Gutowski, M. Carcenac, D. Pourquier, C. Larroque, B. Saint-Aubert, P. Rouanet, A. Pèlegrin, Intraoperative immunophotodetection for radical resection of cancers: evaluation in an experimental model, *Clin. Cancer Res. Off. J. Am. Assoc. Cancer Res.* 7 (2001) 1142–1148.
- [25] A. Leconte, V. Garambois, M. Ychou, B. Robert, D. Pourquier, A. Terskikh, J.P. Mach, A. Pèlegrin, Involvement of circulating CEA in liver metastases from colorectal cancers re-examined in a new experimental model, *Br. J. Cancer* 80 (1999) 1373–1379.
- [26] M.C. Boonstra, B. Tolner, B.E. Schaafsma, L.S.F. Boogerd, H.A.J.M. Prevo, G. Bhavsar, P.J.K. Kuppen, C.F.M. Sier, B.A. Bonsing, J.V. Frangioni, C.J.H. van de Velde, K.A. Chester, A.L. Vahrmeijer, Preclinical evaluation of a novel CEA-targeting near-infrared fluorescent tracer delineating colorectal and pancreatic tumors, *Int. J. Cancer J. Int. Cancer* 137 (2015) 1910–1920, <http://dx.doi.org/10.1002/ijc.29571>.
- [27] H. Kim, K.D. Folks, L. Guo, J.C. Sellers, N.S. Fineberg, C.R. Stockard, W.E. Grizzle, D.J. Buchsbaum, D.E. Morgan, J.F. George, K.R. Zinn, Early therapy evaluation of combined cetuximab and irinotecan in orthotopic pancreatic tumor xenografts by dynamic contrast-enhanced magnetic resonance imaging, *Mol. Imaging* 10 (2011) 153–167.
- [28] M. Berger, F. Cailler, J. Chambron, J.L. Coll, V. Garambois, M. Gutowski, V. Guyon, A. Pèlegrin, F. Scherninski, H. Simon, A. Kazandjian, Vectors and instrumentation for per-operative imaging, *Irbm* 31 (2010) 78–81, <http://dx.doi.org/10.1016/j.irbm.2010.02.008>.
- [29] E.L. Rosenthal, J.M. Warram, E. de Boer, J.P. Basilon, M.A. Biel, M. Bogyo, M. Bouvet, B.E. Brigman, Y.L. Colson, S.R. DeMeester, G.C. Gurtner, T. Ishizawa, P.M. Jacobs, S. Keereweer, J.C. Liao, Q.T. Nguyen, J.M. Olson, K.D. Paulsen, D. Rieves, B.D. Sumer, M.F. Tweedle, A.L. Vahrmeijer, J.P. Weichert, B.C. Wilson, M.R. Zenn, K.R. Zinn, G.M. van Dam, Successful translation of fluorescence navigation during oncologic surgery: a consensus report, *J. Nucl. Med. Off. Publ. Soc. Nucl. Med.* 57 (2016) 144–150, <http://dx.doi.org/10.2967/jnumed.115.158915>.
- [30] S. Keereweer, P.B.A.A. Van Driel, T.J.A. Snoeks, J.D.F. Kerrebijn, R.J. Baatenburg de Jong, A.L. Vahrmeijer, H.J.C.M. Sterenborg, C.W.G.M. Löwik, Optical image-guided cancer surgery: challenges and limitations, *Clin. Cancer Res. Off. J. Am. Assoc. Cancer Res.* 19 (2013) 3745–3754, <http://dx.doi.org/10.1158/1078-0432.CCR-12-3598>.
- [31] A.V. DSouza, H. Lin, E.R. Henderson, K.S. Samkoe, B.W. Pogue, Review of fluorescence guided surgery systems: identification of key performance capabilities beyond indocyanine green imaging, *J. Biomed. Opt.* 21 (2016) 80901, <http://dx.doi.org/10.1117/1.JBO.21.8.08901>.
- [32] C.A. Metildi, S. Kaushal, C.S. Snyder, R.M. Hoffman, M. Bouvet, Fluorescence-guided surgery of human colon cancer increases complete resection resulting in cures in an orthotopic nude mouse model, *J. Surg. Res.* 179 (2013) 87–93, <http://dx.doi.org/10.1016/j.jss.2012.08.052>.
- [33] C.A. Metildi, S. Kaushal, M. Pu, K.A. Messer, G.A. Luiken, A.R. Moossa, R.M. Hoffman, M. Bouvet, Fluorescence-guided surgery with a fluorophore-conjugated antibody to carcinoembryonic antigen (CEA), that highlights the tumor, improves surgical resection and increases survival in orthotopic mouse models of human pancreatic cancer, *Ann. Surg. Oncol.* (2014), <http://dx.doi.org/10.1245/s10434-014-3495-y>.
- [34] J.M. Reichert, Antibodies to watch in 2016, *mAbs* 8 (2016) 197–204, <http://dx.doi.org/10.1080/19420862.2015.1125583>.
- [35] J.P. Mach, S. Carrel, M. Forni, J. Ritschard, A. Donath, P. Alberto, Tumor localization of radiolabeled antibodies against carcinoembryonic antigen in patients with carcinoma: a critical evaluation, *N. Engl. J. Med.* 303 (1980) 5–10 doi:7189578.
- [36] D.M. Goldenberg, F. DeLand, E. Kim, S. Bennett, F.J. Primus, J.R. van Nagell Jr., N. Estes, P. DeSimone, P. Rayburn, Use of radiolabeled antibodies to carcinoembryonic antigen for the detection and localization of diverse cancers by external photoscanning, *N. Engl. J. Med.* 298 (1978) 1384–1386, <http://dx.doi.org/10.1056/NEJM197806222982503>.
- [37] M. Ychou, D. Azria, C. Menkarios, P. Faurois, F. Quenet, B. Saint-Aubert, P. Rouanet, M. Pélegren, C. Bascoul-Mollevi, D. Guerreau, J.-C. Saccavini, J.-P. Mach, J.-C. Artus, A. Pélegren, Adjuvant radioimmunotherapy trial with iodine-131-labeled anti-carcinoembryonic antigen monoclonal antibody F6 F(ab')2 after resection of liver metastases from colorectal cancer, *Clin. Cancer Res. Off. J. Am. Assoc. Cancer Res.* 14 (2008) 3487–3493 doi:7189578.
- [38] P.-Y. Salaun, L. Campion, C. Bournaud, A. Faivre-Chauvet, J.-P. Vuillez, D. Taieb, C. Ansquer, C. Rousseau, F. Borson-Chazot, S. Bardet, A. Oudoux, B. Cariou, E. Mirallié, C.-H. Chang, R.M. Sharkey, D.M. Goldenberg, J.-F. Chatal, J. Barbet, F. Kraeber-Bodéré, Phase II trial of anticarcinoembryonic antigen pretargeted radioimmunotherapy in progressive metastatic medullary thyroid carcinoma: biomarker response and survival improvement, *J. Nucl. Med. Off. Publ. Soc. Nucl. Med.* 53 (2012) 1185–1192, <http://dx.doi.org/10.2967/jnumed.111.101865>.
- [39] J.P. Tiernan, S.L. Perry, E.T. Verghese, N.P. West, S. Yeluri, D.G. Jayne, T.A. Hughes, Carcinoembryonic antigen is the preferred biomarker for *in vivo* colorectal cancer targeting, *Br. J. Cancer* 108 (2013) 662–667, <http://dx.doi.org/10.1038/bjc.2012.605>.
- [40] M.C. Boonstra, S.W.L. de Geus, H.A.J.M. Prevo, L.J.A.C. Hawinkels, C.J.H. van de Velde, P.J.K. Kuppen, A.L. Vahrmeijer, C.F.M. Sier, Selecting targets for tumor imaging: an overview of cancer-associated membrane proteins, biomark, *Cancer* 8 (2016) 119–133, <http://dx.doi.org/10.4137/BIC.S38542>.
- [41] J.V. Frangioni, New technologies for human cancer imaging, *J. Clin. Oncol. Off. J. Am. Soc. Clin. Oncol.* 26 (2008) 4012–4021, <http://dx.doi.org/10.1200/JCO.2007.14.3065>.
- [42] M. Dorvillius, V. Garambois, D. Pourquier, M. Gutowski, P. Rouanet, J.-C. Mani, M. Pugnière, N.E. Hynes, A. Pèlegrin, Targeting of human breast cancer by a bispecific antibody directed against two tumour-associated antigens: Erbb-2 and carcinoembryonic antigen, *Tumour Biol. J. Int. Soc. Oncodevelopmental Biol. Med.* 23 (n.d.) 337–347.
- [43] C.M. O'Kelly Priddy, V.A. Forte, J.E. Lang, The importance of surgical margins in breast cancer, *J. Surg. Oncol* 113 (2016) 256–263, <http://dx.doi.org/10.1002/jso.24047>.
- [44] E.A. Owens, M. Henary, G. El Fakhri, H.S. Choi, Tissue-specific near-infrared fluorescence imaging, *Acc. Chem. Res.* (2016), <http://dx.doi.org/10.1021/acs.accounts.6b00239>.
- [45] C. Ortega, A. Herbet, S. Richard, N. Kersual, N. Costa, A. Pèlegrin, F. Ducancel, J.-Y. Couraud, I. Navarro-Teulon, D. Boquet, High level prokaryotic expression of anti-Müllerian inhibiting substance type II receptor diabody, a new recombinant antibody for *in vivo* ovarian cancer imaging, *J. Immunol. Methods* (2012), <http://dx.doi.org/10.1016/j.jimm.2012.08.003>.
- [46] P.B.A.A. van Driel, J.R. van der Vorst, F.P.R. Verbeek, S. Oliveira, T.J.A. Snoeks, S. Keereweer, B. Chan, M.C. Boonstra, J.V. Frangioni, P.M.P. van Bergen en Henegouwen, A.L. Vahrmeijer, C.W.G.M. Lowik, Intraoperative fluorescence delineation of head and neck cancer with a fluorescent anti-epidermal growth factor receptor nanobody, *Int. J. Cancer J. Int. Cancer* 134 (2014) 2663–2673, <http://dx.doi.org/10.1002/ijc.28601>.
- [47] T. Kruwel, D. Nevoltris, J. Bode, C. Dullin, D. Baty, P. Chames, F. Alves, *In vivo* detection of small tumour lesions by multi-pinhole SPECT applying a (99m) Tc-labelled nanobody targeting the Epidermal Growth Factor Receptor, *Sci. Rep.* 6 (2016) 21834, <http://dx.doi.org/10.1038/srep21834>.
- [48] Y. Urano, M. Sakabe, N. Kosaka, M. Ogawa, M. Mitsunaga, D. Asanuma, M. Kamiya, M.R. Young, T. Nagano, P.L. Choyke, H. Kobayashi, Rapid cancer detection by topically spraying a γ -glutamyltranspeptidase-activated fluorescent probe, *Sci. Transl. Med.* 3 (2011), <http://dx.doi.org/10.1126/scitranslmed.3002823>, 110ra119.
- [49] A.M. Cuesta, N. Sainz-Pastor, J. Bonet, B. Oliva, L. Alvarez-Vallina, Multivalent antibodies: when design surpasses evolution, *Trends Biotechnol.* 28 (2010) 355–362, <http://dx.doi.org/10.1016/j.tibtech.2010.03.007>.
- [50] S. Reagan-Shaw, M. Nihal, N. Ahmad, Dose translation from animal to human studies revisited, *FASEB J. Off. Publ. Fed. Am. Soc. Exp. Biol.* 22 (2008) 659–661, <http://dx.doi.org/10.1096/fj.07-9574LSF>.
- [51] E.L. Rosenthal, J.M. Warram, E. de Boer, T.K. Chung, M.L. Korb, M. Brandwein-Gensler, T.V. Strong, C.E. Schmalbach, A.B. Morlandt, G. Agarwal, Y.E. Hartman, W.R. Carroll, J.S. Richman, L.K. Clemons, L.M. Nabell, K.R. Zinn, Safety and tumor specificity of cetuximab-IRDye800 for surgical navigation in head and neck cancer, *Clin. Cancer Res. Off. J. Am. Assoc. Cancer Res.* 21 (2015) 3658–3666, <http://dx.doi.org/10.1158/1078-0432.CCR-14-3284>.